Neutron diffuse scattering in the plastic phase of succinonitrile

1990 J. Phys.: Condens. Matter 2 9975

(http://iopscience.iop.org/0953-8984/2/50/002)

J. Phys.: Condens. Matter **2** (1990) 9975–9987. Printed in the UK

Neutron diffuse scattering in the plastic phase of succinonitrile

P Derollez†‖, J Lefebvre†, M Descamps†, W Press‡ and H Grimm§

† Laboratoire de Dynamique des Cristaux Moléculaires (Unité de Recherche associée au CNRS 801), Université des Sciences et Techniques de Lille Flandres Artois, 59655 Villeneuve d'Ascq Cédex, France

‡ Institut für Experimentalphysik der Universität Kiel, D2300 Kiel 1, Federal Republic of Germany

§ Institut für Festkörperforschung, Kernforschungsanlage Jülich, D5170 Jülich, Federal Republic of Germany

Received 17 May 1990, in final form 21 September 1990

Abstract. Experimental results on neutron quasi-elastic diffuse scattering in the plastic phase of 99% deuterated succinonitrile are reported. Very strong correlations of steric origin occur between orientationally disordered molecules. Their influence on the diffuse scattering is analysed by a mean-field treatment of the hard-core repulsions.

1. Introduction

Scattering from plastic (orientationally disordered) phases is characterized by a limited number of Bragg diffraction peaks and a large diffuse scattering intensity. The latter reflects the disorder and frequently has considerable structure due to orientational molecular correlations. It is this aspect that we shall analyse in the particular case of succinonitrile. The Bragg diffraction analysis of succinonitrile has been reported in a recent paper [1]. The present study describes measurements of the diffuse scattering which provides supplementary information about the succinonitrile system. In earlier studies, one of us has shown that the correlations of steric origin are an essential feature of the plastic phase [2–4]. The static scattering cross section has been calculated from a series expansion to include correlations between second-nearest-neighbour molecules. The second-nearest-neighbour correlations were considered as being the most important for determining the structure of the diffuse scattering. Using a simplified model of interactions and structural results known at that time, the cross section including correlations leads to good agreement with experimental x-ray data for particular directions in reciprocal space. One of the objectives of this paper is to reconsider this theoretical analysis based on more complete structural results by comparison with the present neutron diffuse scattering measurements.

At room temperature, succinonitrile $N{\equiv}C{-}(CH_2)_2{-}C{\equiv}N$ crystallizes in the Im3m space group with two molecules per unit cell. X-ray diffraction and Raman scattering

‖ Present address: Institut Laue-Langevin, 156X, 38042 Grenoble Cédex, France.

0953-8984/90/509975 + 13 $03.50

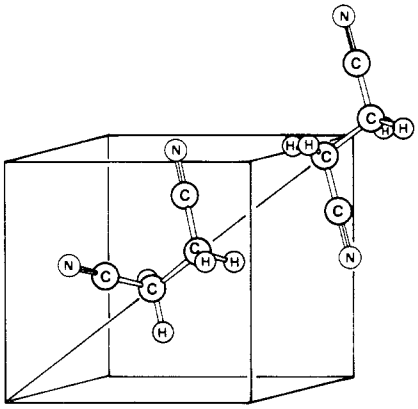

Figure 1. Schematic drawing for *gauche* and *trans* isomers in the cubic cell.

experiments [4–7] have revealed that the molecule can assume three isomeric forms: one *trans* and two *gauche* conformations. In the former, the nitrile groups are in the symmetry plane of the molecule. The latter are obtained from the *trans* conformation by relative rotations of $\pm 120°$ of one nitrile group relative to the other around the central C—C bond. This central C—C bond is preferentially aligned along the four threefold axes of the cubic cell. Each nitrile group can occupy three equilibrium positions which are obtained by rotations of 120° around the threefold axis (see figure 1).

Experiments using NMR [8], dielectric relaxation [9], Rayleigh scattering [10] and incoherent neutron scattering [11–13] have revealed dynamic orientational disorder of the molecules.

(i) For rotational jumps of the whole molecule around a fourfold axis, the central C—C bond aligns itself along another threefold axis of the cell.

(ii) For rotations of CH_2—C≡N groups around a threefold axis, one isomer is changed into another.

Each isomer has 12 orientational configurations in the lattice. Because of the three different isomers, the molecule can adopt 36 equilibrium configurations.

From our more extended x-ray diffraction measurements [1], we have deduced the translation–rotation coupling in the disordered phase. It was shown that the coupling is directly related to the spatial siting of neighbouring molecules and that it affects the positions of the *gauche* isomers. An offset parameter along the twofold axes was introduced in the refinement procedure which brings the centre of mass of the *gauche* conformations back towards the molecular site. It was found to have an amplitude of 0.42 Å. The analysis of the spatial siting of neighbour molecules has revealed that the steric effects involve strong local correlations which explain the large value of the offset parameter.

2. Experimental details

The single crystal of deuterated succinonitrile was produced with a growth rate of 0.5 mm h^{-1} by the Bridgman–Stockbarger technique. Neutron diffuse scattering experiments were performed on the triple-axis spectrometer, SV4, at Kernforschungsanlage Jülich

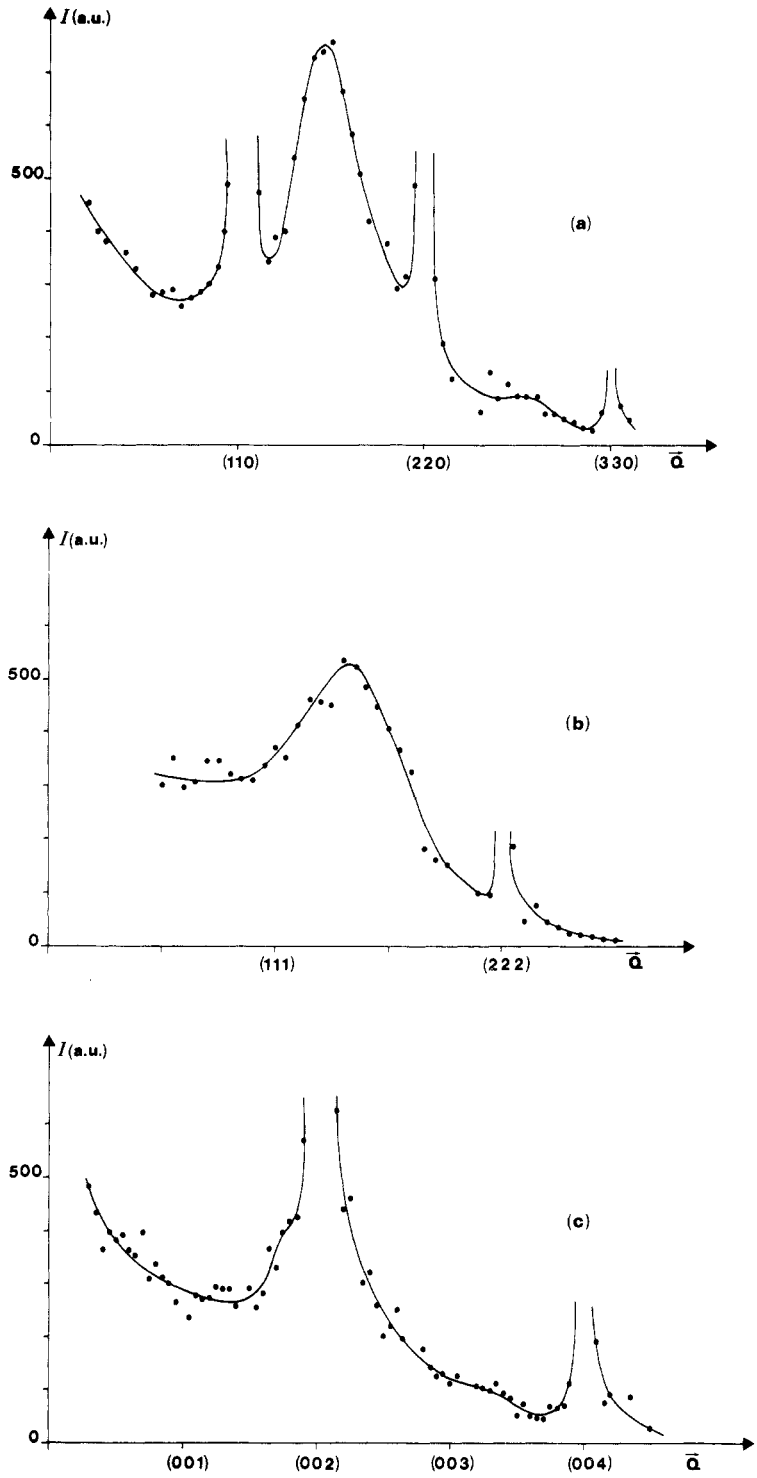

Figure 2. Experimental neutron diffuse scattering at $T = 295$ K for Q along the three principal directions (*a*) $[110]^*$, (*b*) $[111]^*$ and (*c*) $[001]^*$.

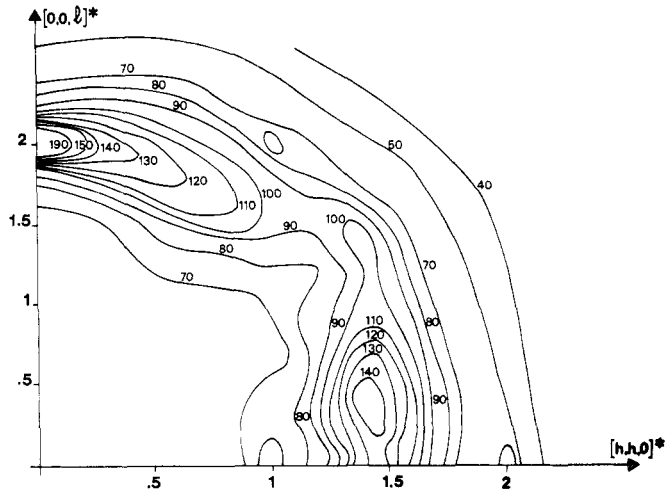

Figure 3. Experimental neutron diffuse scattering contour map in the $(1\bar{1}0)^*$ plane at $T = 295$ K.

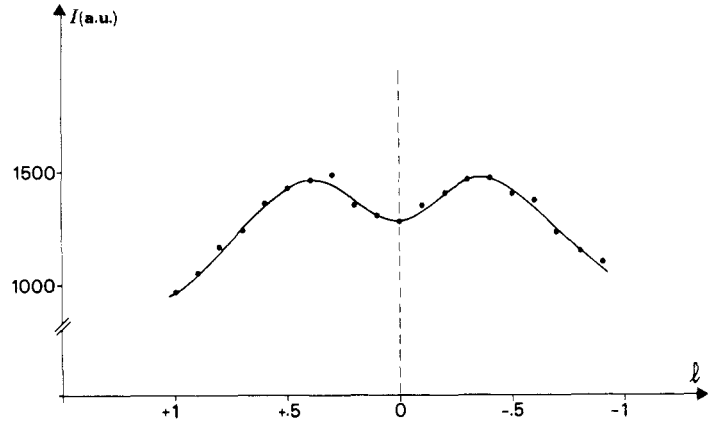

Figure 4. Experimental diffuse scattering along the $[1.40, 1.40, l]^*$ direction at $t = 295$ K.

(Federal Republic of Germany). A pyrolitic graphite double monochromator selected an incident wavelength λ_i of 2.36 Å and a graphite crystal analysed the scattered beam. This arrangement gave an energy resolution of about 1 meV (FWHM). The sample, wrapped in aluminium foil, was placed in a nitrogen cryostat. The measured intensities were corrected for sample environment.

2.1. Diffuse scattering at T = 295 K

The quasi-elastic scattering at $T = 295$ K along the three principal reciprocal space directions is shown in figure 2. For scattering vectors $\boldsymbol{Q}$ along the $[110]^*$ direction (figure 2(*a*)), the diffuse intensity shows a pronounced maximum around $\boldsymbol{Q} = (1.45, 1.45, 0)$,

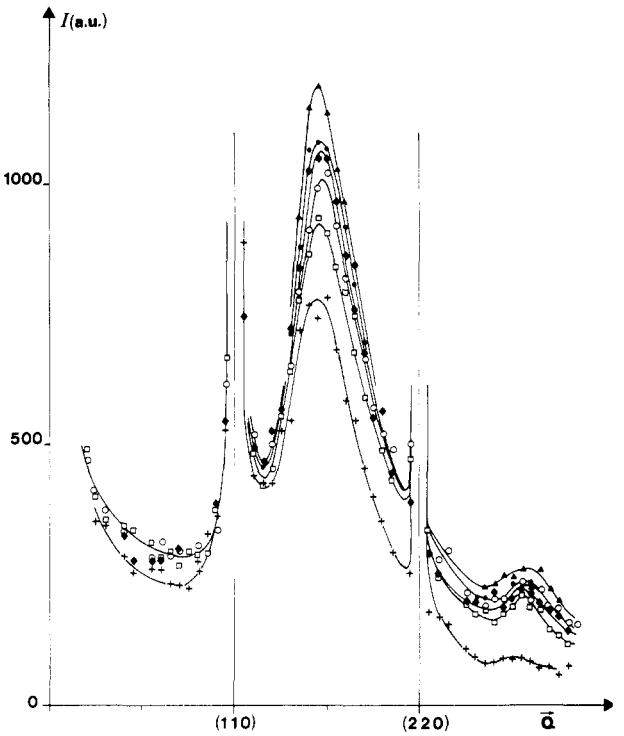

Figure 5. Experimental diffuse scattering at different temperatures for $\boldsymbol{Q}$ along the [110]* direction: +, 295 K; □, 251 K; ○, 240 K; ◆, 235 K; ●, 229 K; ▲, 219 K.

between the diffraction peaks. A less intense maximum is also observed at about $\boldsymbol{Q}$ = (2.5, 2.5, 0). The diffuse scattering for $\boldsymbol{Q}$ along [111]* (figure 2(*b*)) shows a large bump of lower intensity whose maximum is around (1.35, 1.35, 1.35). For $\boldsymbol{Q}$ along the [001]* direction (figure 2(*c*)), the diffuse scattering peak is obscured by the (002) diffraction peak. The relative intensities and positions of the maxima are in agreement with the x-ray scattering results of Descamps [2, 4] for the hydrogenated compound.

Scans were also performed in the $(1\bar{1}0)^*$ plane and at $T = 295$ K. Figure 3 shows contours of constant intensity obtained from about 1650 measured points. The scattered intensity is modulated on a ring of mean radius 2 Å^{-1}. The maxima are notably very close to the twofold and threefold axes. A particularly intense scattering peak appears near [110]* for $\boldsymbol{Q}$ = (1.40, 1.40, 0.40). The position of this maximum was checked more carefully by performing a further scan along the [1.40, 1.40, l]* direction shown in figure 4.

2.2. *Variation in the diffuse scattering as a function of the temperature*

The scattering for $\boldsymbol{Q}$ along [110]* is shown in figure 5 for the temperature range from $T = 295$ K to $T = 219$ K. The diffuse scattering increases gradually as the temperature decreases but no pretransitional effect is detected. The equilibrium first ordering transition occurs at $T = 233$ K but the high-temperature plastic phase can be easily supercooled, allowing measurements in the plastic phase down to $T = 219$ K. The

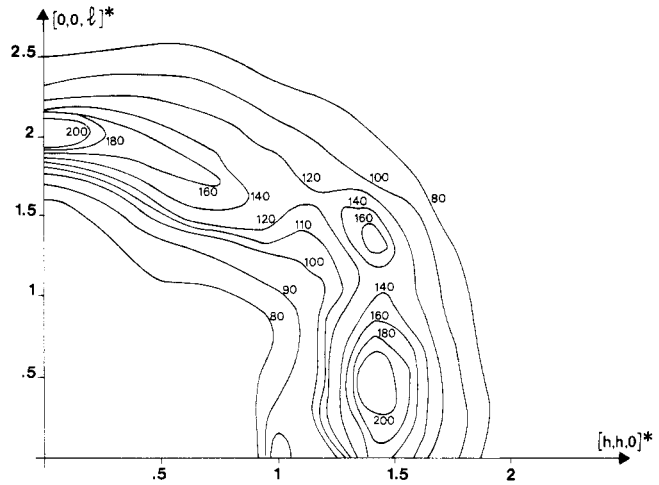

Figure 6. Experimental scattering contour map in the $(1\bar{1}0)^*$ plane at $T = 234$ K.

intensity contours for the $(1\bar{1}0)^*$ plane at $T = 234$ K are shown in figure 6 and are similar to those at 295 K. The scattered intensity is found to vary as a Debye–Waller factor.

3. Intermolecular correlations: mean-field treatment of the hard-core repulsions

3.1. Theoretical principle

Let us recall here the principle of the mean-field calculation method which is especially suited to the study of correlations of steric origin. The method has been developed in detail elsewhere [14, 15] and only a summary of the different stages of the calculation of the static neutron cross section is given here. The calculation allows an analysis of the influence of the interactions of steric origin due to the first-neighbour molecules as well as the second-neighbour molecules on the diffuse scattering.

For steric hindrances, it is convenient to use a compatibility function taking the values 1 or 0 for orientationally compatible or non-compatible neighbours, respectively. For steric effects, the mean-field approximation assumes that the molecule at the site i (orientation Ω^i) is governed, in the (ij) direction, by an average compatibility function which may be written

$$A_{ij}(\Omega^i) = \begin{cases} 1 & \text{if the orientation } \Omega^i \text{ of the molecule at the site } i \text{ is compatible with all the possible orientations of the molecule at the site } j \\ 1 - \lambda_j \langle C_{ij} \rangle & \text{otherwise} \end{cases} \tag{1}$$

where $\langle C_{ji} \rangle$ denotes the average occupation rate of the (ji) direction by the j molecule. The coefficient λ_j $(0 < \lambda_j < 1)$ is an index of the extent of relaxation of the repulsions. If we characterize the orientations actually occupied by the function

Table 1. Molecular orientations l and corresponding positions of the nitrogen atoms. The atomic coordinates are given in [1]. e is the offset parameter for *gauche* isomers.

l	Positions of the nitrogen atoms					
1	x	x	z	$-x$	$-x$	$-z$
2	z	x	x	$-z$	$-x$	$-x$
3	x	z	x	$-x$	$-z$	$-x$
4	x	$-x$	$-z$	$-x$	x	z
5	z	$-x$	$-x$	$-z$	x	x
6	x	$-z$	$-x$	$-x$	z	x
7	$-x$	x	$-z$	x	$-x$	z
8	$-z$	x	$-x$	z	$-x$	x
9	$-x$	z	$-x$	x	$-z$	x
10	$-x$	$-x$	z	x	x	$-z$
11	$-z$	$-x$	x	z	x	$-x$
12	$-x$	$-z$	x	x	z	$-x$
13	x	$x+e$	$z-e$	$-x$	$-z+e$	$-x-e$
14	$z-e$	x	$x+e$	$-x-e$	$-x$	$-z+e$
15	$x+e$	$z-e$	x	$-z+e$	$-x-e$	$-x$
16	x	$-x-e$	$-z+e$	$-x$	$z-e$	$x+e$
17	$z-e$	$-x$	$-x-e$	$-x-e$	x	$z-e$
18	$x+e$	$-z+e$	$-x$	$-z+e$	$x+e$	x
19	$-x$	$x+e$	$-z+e$	x	$-z+e$	$x+e$
20	$-z+e$	x	$-x-e$	$x+e$	$-x$	$z-e$
21	$-x-e$	$z-e$	$-x$	$z-e$	$-x-e$	x
22	$-x$	$-x-e$	$z-e$	x	$z-e$	$-x-e$
23	$-z+e$	$-x$	$x+e$	$x+e$	x	$-z+e$
24	$-x-e$	$-z+e$	x	$z-e$	$x+e$	$-x$
25	x	$z-e$	$x+e$	$-x$	$-x-e$	$-z+e$
26	$x+e$	x	$z-e$	$-z+e$	$-x$	$-x-e$
27	$z-e$	$x+e$	x	$-x-e$	$-z+e$	$-x$
28	x	$-z+e$	$-x-e$	$-x$	$x+e$	$z-e$
29	$x+e$	$-x$	$-z+e$	$-z+e$	x	$x+e$
30	$z-e$	$-x-e$	$-x$	$-x-e$	$z-e$	x
31	$-x$	$z-e$	$-x-e$	x	$-x-e$	$z-e$
32	$-x-e$	x	$-z+e$	$z-e$	$-x$	$x+e$
33	$-z+e$	$x+e$	$-x$	$x+e$	$-z+e$	x
34	$-x$	$-z+e$	$x+e$	x	$x+e$	$-z+e$
35	$-x-e$	$-x$	$z-e$	$z-e$	x	$-x-e$
36	$-z+e$	$-x-e$	x	$x+e$	$z-e$	$-x$

$$\mu_l^i = \begin{cases} 1 & \text{if the molecular orientation at the site } i \text{ is } l \\ 0 & \text{if not} \end{cases} \tag{2}$$

then $\langle C_{ji} \rangle$ may be expressed in terms of $\langle \mu_l^i \rangle$.

In the mean-field approximation, the configurational partition function is

$$Z^{\mathrm{MF}} = \sum_{\Omega^i}^{D} \prod_{(ij)}^{q\,\prime} A_{ij}(\Omega^i) \prod_{l}^{D} (b_l^i)^{\mu_l^i}. \tag{3}$$

b_l^i denotes the activity of the ith molecule with the orientation l. The summation and the

Table 2. Indexation of the molecular sites.

Second-neighbour molecules				First-neighbour molecules			
Site indexation	Reduced cordinates			Site indexation	Reduced coordinates		
1	1	0	0	I	$\frac{1}{2}$	$\frac{1}{2}$	$\frac{1}{2}$
2	0	1	0	II	$-\frac{1}{2}$	$-\frac{1}{2}$	$-\frac{1}{2}$
3	0	0	1	III	$-\frac{1}{2}$	$\frac{1}{2}$	$\frac{1}{2}$
4	−1	0	0	IV	$\frac{1}{2}$	$-\frac{1}{2}$	$-\frac{1}{2}$
5	0	−1	0	V	$\frac{1}{2}$	$-\frac{1}{2}$	$\frac{1}{2}$
6	0	0	−1	VI	$-\frac{1}{2}$	$\frac{1}{2}$	$-\frac{1}{2}$
				VII	$\frac{1}{2}$	$\frac{1}{2}$	$-\frac{1}{2}$
				VIII	$-\frac{1}{2}$	$-\frac{1}{2}$	$\frac{1}{2}$

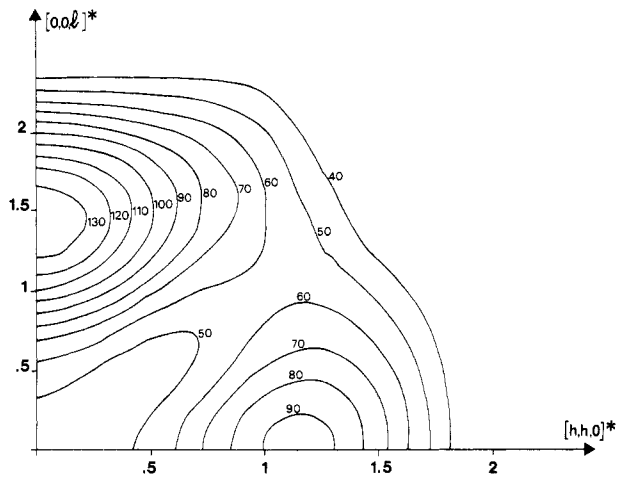

Figure 7. Theoretical neutron intensity contours for the $(1\bar{1}0)^*$ plane at $T = 295$ K. The correlations are not taken into account in the calculation.

second product run over the D orientationally discrete states and the first product is over the q lattice directions from a given site. The average occupation rate $\langle \mu_m^i \rangle$ thus reads

$$\langle \mu_m^i \rangle = b_m^i \frac{\partial}{\partial b_m^i} (\log Z^{\mathrm{MF}}) = (Z^{\mathrm{MF}})^{-1} \sum_{\Omega^i} \mu_m^i \prod_{(ij)}^{q\,\prime} A_{ij}(\Omega^i) \prod_{l}^{D} (b_l^i)^{\mu_l^i}. \tag{4}$$

A perturbation calculation leads to the expression of the diffuse scattering intensity in the following way: we impose a perturbation which varies from one site to another such that

$$\begin{aligned} \langle \mu_l^i \rangle &= \langle \mu_l^i \rangle^{\mathrm{eq}} + \delta \langle \mu_l^i \rangle \\ b_l^i &= b_l^{i\mathrm{eq}} + \delta b_l^i \end{aligned} \tag{5}$$

where $\langle \mu_l^i \rangle^{\mathrm{eq}}$ and $b_l^{i\mathrm{eq}}$ denote the occupation rates and the activities at equilibrium. The

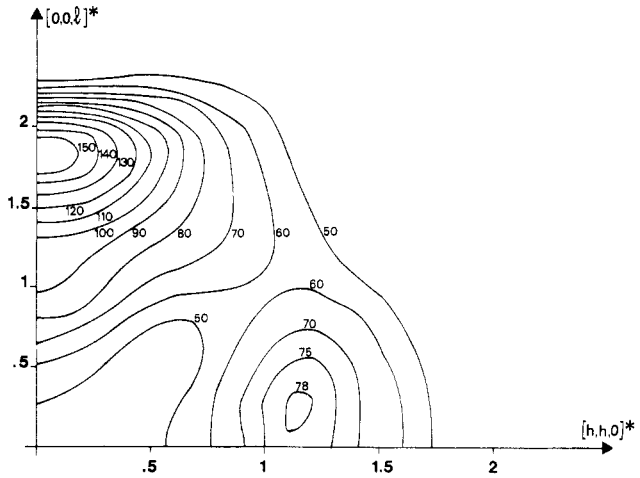

Figure 8. Theoretical intensity contours in the $(1\bar{1}0)^*$ plane at $T = 295$ K including correlations between only second-neighbour molecules.

complete set of consistency equations is thus obtained by Fourier transformation. We define a static susceptibility matrix $\boldsymbol{\chi}(Q)$ $(=D \times D)$ such that

$$\delta\langle\mu(Q)\rangle = \boldsymbol{\chi}(Q)\,\delta g(Q). \tag{6}$$

$\delta\langle\mu(Q)\rangle$ and $\delta g(Q)$ are the Fourier transforms of $\delta\langle\mu_m^i\rangle$ and $\delta b_l^i/b_l^i$, respectively. If we introduce a D-dimensional vector $f(Q)$ whose components are the different form factors of the molecule in its different states, we can write a form factor matrix

$$\mathbf{F}(Q) = f(Q) \otimes f^{\mathrm{adj}}(Q). \tag{7}$$

The diffuse scattering intensity is thus obtained from

$$S_{\mathrm{scatt}}(Q) = N\,\mathrm{Tr}[F^{\mathrm{T}}(Q)\boldsymbol{\chi}(Q)] \tag{8}$$

where N is the number of sites in the crystal, Tr represents the trace and the superscript T implies the transpose.

3.2. Application to succinonitrile

The first stage of the calculation is to determine all the incompatible orientations between a given molecule taken as an origin and its neighbours. It is known that one molecule can adopt 36 distinct orientations on a site. Therefore, taking into account interactions between one molecule and its eight first and six second neighbours, we have to consider $36 \times 36 \times 15$ orientational configurations.

It has been shown [1] that the steric effects due to second-neighbour molecules give rise to 6×144 forbidden configurations. In this case, the overlap of the nitrogen van der Waals spheres is very important: the distance between the nitrogen atoms is between 0.48 and 1.10 Å according to the isomer whereas the van der Waals radius of the nitrogen atom is 1.60 Å. Therefore, all the forbidden configurations were taken into account in the calculation.

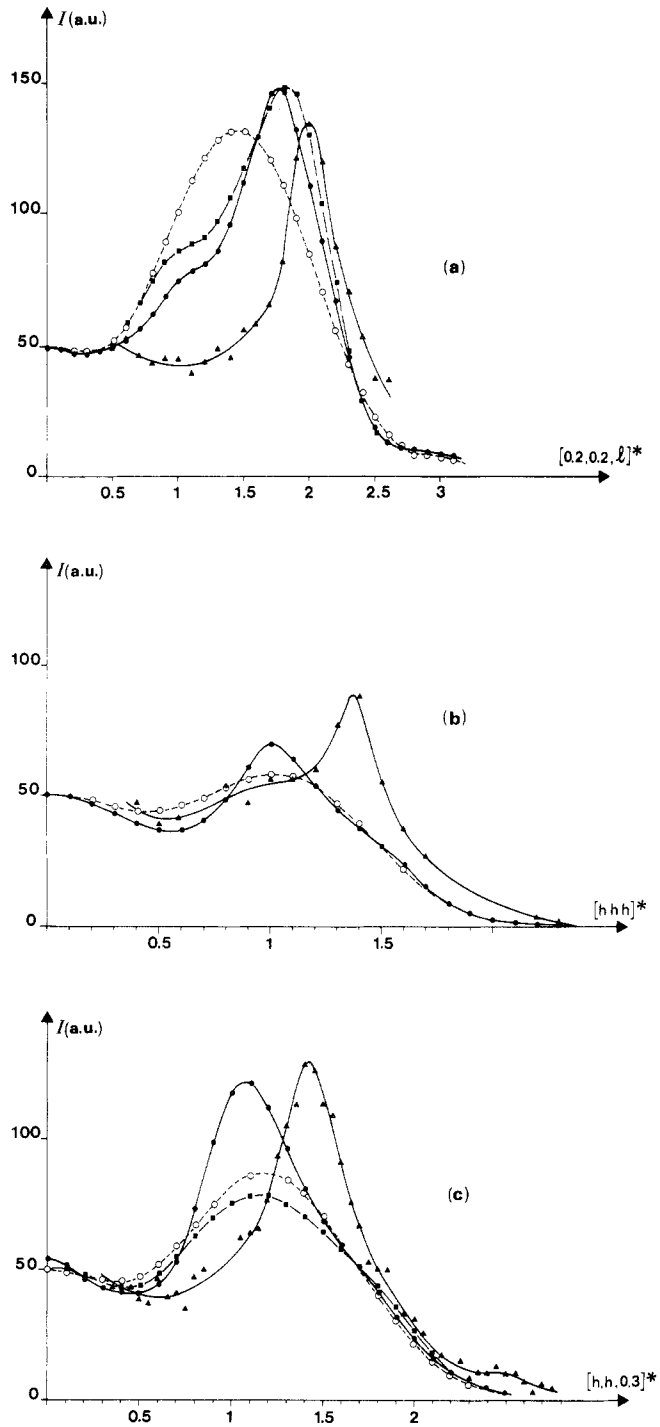

Figure 9. Experimental (▲) and theoretical scattered intensities without correlations (○), including correlations between only second-neighbour molecules (■) and correlations between first- and second-neighbour molecules (●) in the three directions (*a*) $[0.2, 0,2\ l]^*$ (*b*) $[h, h, h]^*$ and (*c*) $[h, h, 0.3]^*$. In (*b*), ■ and ○ are superposed.

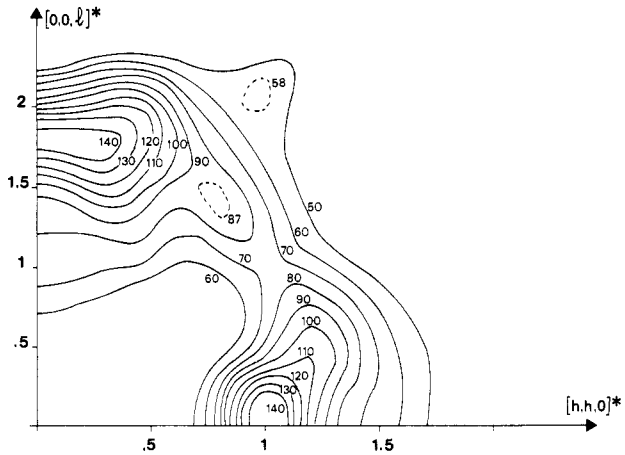

Figure 10. Theoretical intensity contours in the $(1\bar{1}0)^*$ plane at $T = 295$ K including correlations between first- and second-neighbour molecules as mentioned in the text.

Between the first neighbours, the number of hindered configurations is very high (8×444) and overlaps between carbon and nitrogen atoms are also involved. In many cases, the atom–atom overlap is not as important as for second neighbours and the forbidden orientational configurations in the calculation were those which show the strongest overlaps. If d_{12} denotes the distance between the atoms 1 and 2 of neighbour molecules and r_1 and r_2 the corresponding van der Waals radii, then we may assume that there is an effective steric hindrance if $d_{12}/(r_1 + r_2)$ is below 0.95. Moreover, it was shown [1] that the number of hindered configurations is related to the offset parameter. We considered only the case where the steric hindrance was minimized. Under these assumptions, 8×192 of the configurations which involve the strongest hindrance are effectively taken into account in the model.

The different molecular orientations were classified from the positions of the nitrogen atoms in the crystal, as shown in table 1. The molecules with orientation l such that $1 \leqslant l \leqslant 12$ are *trans* isomers whereas those with $13 \leqslant l \leqslant 36$ are *gauche* isomers. The classification of the molecular sites is given in table 2.

We are now able to write the mean compatibility function $A_{0j}(l)$ for each l and each $(0j)$ direction. For example, the compatibility function for first-neighbour sites may be written as

$$A_{0I}(1) = 1 - \lambda_1(\langle\mu^I_{15}\rangle + \langle\mu^I_{24}\rangle + \langle\mu^I_{27}\rangle + \langle\mu^I_{36}\rangle).$$

For second-neighbour sites, we obtain

$$A_{03}(1) = 1 - \lambda_2(\langle\mu^3_1\rangle + \langle\mu^3_4\rangle + \langle\mu^3_7\rangle + \langle\mu^3_{10}\rangle + \langle\mu^3_{14}\rangle + \langle\mu^3_{16}\rangle + \langle\mu^3_{19}\rangle + \langle\mu^3_{23}\rangle + \langle\mu^3_{25}\rangle + \langle\mu^3_{29}\rangle + \langle\mu^3_{32}\rangle + \langle\mu^3_{34}\rangle).$$

The configurational partition and the expectation values of the orientations in the mean-field approximation may be determined from equations (3) and (4). The next step is the expression of the fluctuations of 36 occupation rates which are given by the coupled equations derived from equation (5).

The relative activities of the *trans* isomers with respect to those of the *gauche* isomers are defined by

$$b_l^{eq} = \xi \qquad (1 \leqslant l \leqslant 12).$$

The 36 coupled equations can be solved by Fourier transform, yielding the partition function for the system at equilibrium as

$$Z_{eq}^{MF} = (1-\lambda_2/3)^2\{12\xi[1-\lambda_1(1-\rho_t)/6]^8 + 24[1-\lambda_1(3\rho_t+7)/24]^4\}.$$

ξ is related to the proportion of the *trans* isomer by

$$\rho_t = \xi\,(\partial/\partial\xi)\,(\log Z_{eq}^{MF}) = \xi/(\xi + 2\eta) \tag{9}$$

with $\eta = (\frac{3}{2})^4[24-\lambda_1(3\rho_t+7)]^4/[6-\lambda_1(1-\rho_t)]^8$. From equation (9), ξ is given by $\xi = 2\rho_t\eta/(1-\rho_t)$.

ξ gives a measure of the influence of the correlations on the proportion of isomers. In the calculation, we have used the value of ξ which was deduced from the experimental proportion $\rho_t = 23\%$ of *trans* isomers [7] and including the correlations of our model. In this way, when there is no correlation ($\lambda_1 = 0$), ξ reduces to a value corresponding to a random mixing $\xi = 2\rho_t/(1-\rho_t)$. However, for maximum correlation ($\lambda_1 = 1$) as is the case in this study, the experimental value of ρ_t gives a ξ-value of 0.38.

4. Discussion

The scattered intensity was calculated by assuming that the temperature factors of the deuterated sample were proportional to those of the hydrogenated sample, the coefficient of proportionality being the ratio of the molecular masses of the two compounds. The sample was 99% deuterated and the incoherent scattering was negligible with respect to the coherent scattering for $|\boldsymbol{Q}| > 1.40$ Å^{-1}.

As a first approximation and for comparison, the diffuse scattering was calculated by neglecting the intermolecular correlations. The resulting equi-intensity contours in the $(1\bar{1}0)^*$ plane are shown in figure 7. In this approximation, the predicted scattering appears to be more diffuse than the measured scattering is and the positions of the maxima are also incorrect. It is therefore important to introduce the orientational incompatibilities.

To build the model, we have used the structural results of [1] and the steric hindrance as mentioned in the above paragraph. The scattered intensity which takes into account only the interactions between the second-neighbour molecules is shown in figure 8. The results are in good agreement with the data near the $[001]^*$ direction but do not describe correctly the observed intensities in the $(1\bar{1}0)^*$ plane. Therefore, correlations with first-neighbour molecules were introduced. Figure 9 shows the experimental and theoretical scattering intensities in three reciprocal space directions. For $\boldsymbol{Q}$ along $[0.2, 0.2, l]^*$ (figure 9(*a*)), the introduction of the first-neighbour correlations gives a noticeably better agreement with the experimental data. For $\boldsymbol{Q}$ along $[h, h, 0.3]^*$ (figure 9(*c*)), the relative intensities are well described by the model although the positions of the maxima are not well predicted. The corresponding isoscattering contours are shown in figure 10. The main deviation of the experimental scattering from the model exists around the $[110]^*$ direction. However, the introduction of intermolecular correlations of steric origin provides a qualitative improvement. By including correlations between first neighbours, there is better agreement with the experimental intensities, and especially the contrast,

but this is still insufficient for explaining the positions of the observed maxima, in particular along the [110]* direction.

To improve the calculation, we can foresee several possibilities. Up to now, the diffuse scattering has been calculated using the Frenkel model which assumes that the molecules are distributed on discrete equilibrium orientations. A continuous orientational probability distribution could be another way to study the influence of the local order on the diffuse scattering. It also appears that the width of the experimental scattering peak along the [0.2, 0.2, l]* direction is much narrower than the calculated one (figure 9(a)). This is indicative of the presence of longer-range correlations which are excluded in the present calculation. We have shown that the introduction of steric effects between first neighbours (which is the originality of our model) cannot give a complete interpretation of the diffuse scattering. A next step would be to include interactions of longer range (essentially dipolar).

References

[1] Derollez P, Lefebvre J, Descamps M, Press W and Fontaine H 1990 *J. Phys.: Condens. Matter* **2** 6893
[2] Descamps M 1974 *Solid State Commun.* **14** 77
[3] Coulon G and Descamps M 1980 *J. Phys. C: Solid State Phys.* **13** 945
[4] Descamps M 1978 Thèse de Doctorat d'Etat, Lille
[5] Fontaine H and Bée M 1972 *Bull. Soc. Fr. Minéral. Cristallogr.* **95** 441
[6] Fontaine H, Longueville W and Wallart F 1971 *J. Chim. Physique* **68** 1953
[7] Fontaine H 1973 Thèse de Doctorat d'Etat, Lille
[8] Powles J G, Begum A and Norris M O 1969 *Mol. Phys.* **17** 489
[9] Longueville W, Fontaine H and Chapoton A 1971 *J. Chim. Physique* **68** 436
[10] Boyer L, Vacher R, Cecchi L, Adam M and Berge P 1971 *Phys. Rev. Lett.* **26** 1435
[11] Lechner R E, Amoureux J P, Bée M and Fouret R 1977 *Commun. Phys.* **2** 207
[12] Amoureux J P, Bée M, Fouret R and Lechner R E 1977 *Neutron Inelastic Scattering* vol 1 (Vienna: International Atomic Energy Agency) p 397
[13] Bée M, Amoureux J P and Lechner R E 1980 *Mol. Phys.* **4** 945
[14] Descamps M and Coulon G 1981 *J. Phys. C: Solid State Phys.* **14** 2297
[15] Descamps M 1982 *J. Phys. C: Solid State Phys.* **15** 7265